EUROPEAN FUSION DEVELOPMENT AGREEMENT

EFDA–JET–CP(02)01/13

R.A. Pitts, P. Andrew, Y. Andrew, M. Becoulet, I. Coffey, D. Coster, D.C. McDonald, T. Eich, S.K. Erents, M. E. Fenstermacher, W. Fundamenski, G. Haas, A. Hermann, C. Hidalgo, D. Hillis, A. Huber, L.C. Ingesson, S. Jachmich, A. Kallenbach, A. Korotkov, K. Lawson, P. Lomas, T. Loarer, A. Loarte, G.F. Matthews, G.McCracken, A. Meigs, Ph. Mertens, M. O'Mullane, V. Philipps, G. Porter, A. Pospieszczyk, J. Rapp, D. Reiter, V. Riccardo, G. Saibene, R. Sartori, M.F. Stamp, E. Tsitrone and M. Wischmeier

Comparing Scrape-Off-Layer and Divertor Physics in JET Pure He and D Discharges

Comparing Scrape-Off-Layer and Divertor Physics in JET Pure He and D Discharges

R. A. Pitts[1], P. Andrew[2], Y. Andrew[2], M. Becoulet[10], I. Coffey[2], D. Coster[3], D. C. McDonald[2],T. Eich[3], S. K. Erents[2], M. E. Fenstermacher[4], W. Fundamenski[2], G. Haas[3], A. Hermann[3], C. Hidalgo[5], D. Hillis[6], A. Huber[7], L. C. Ingesson[11], S. Jachmich[8], A. Kallenbach[3], A. Korotkov[2], K. Lawson[2], P. Lomas[2], T. Loarer[10], A. Loarte[9], G. F. Matthews[2], G. McCracken[2], A. Meigs[2], Ph. Mertens[7], M. O'Mullane[2], V. Philipps[8], G. Porter[4], A. Pospieszczyk[7], J. Rapp[7], D. Reiter[7], V. Riccardo[2], G. Saibene[9], R. Sartori[9], M. F. Stamp[2], E. Tsitrone[10], M. Wischmeier[1] and contributors to the EFDA-JET workprogramme*

[1]Centre de Recherches en Physique des Plasmas, Association EURATOM-Conf dération Suisse, Ecole Polytechnique Fédérale de Lausanne, CH-1015 Lausanne, Switzerland
[2]Euratom/UKAEA Fusion Association, Culham Science Centre, Abingdon, Oxon. OX14 3DB, UK
[3]Max-Planck-Institut für Plasmaphysik, EURATOM-Association, Boltzmann Str. 2., D-85748, Garching, Germany
[4]Lawrence Livermore National Laboratory, Livermore, CA 94551, USA
[5]Asociaci n EURATOM-CIEMAT, 28040 Madrid, Spain
[6]Oak Ridge National Laboratory, Oak Ridge, TN, USA
[7]FZJ Julich GmbH/Euratom Institut für Plasmaphysik, TEC, Julich D-52425 Germany
[8]LPP, ERM/KMS, Association Euratom-Belgian State, B-1000, Brussels, Belgium
[9]EFDA-CSU, Max-Planck-Institut für Plasmaphysik, D-85748, Garching Germany
[10]Association EURATOM-CEA, CEA Cadarache, 13018 St. Paul lez Durance, France.
[11]FOM-Rijnhuizen, Association Euratom-FOM, TEC, PO Box 1207, Nieuwegein 3430 BE, Netherlands
**See annex of J. Pamela et al., "Overview of recent JET results and Future Perspectives", Fusion Energy 2000 (Proc. 18th Int. Conf. Sorrento, 2000), IAEA Vienna (2001)*

Preprint of Paper to be submitted for publication in
Proceedings of the 15th PSI Conference, (GIFU, Japan 22-31 May 2002)

ABSTRACT

Though Helium plasmas are one option for the low activation phase of ITER, little effort has thus far been devoted to studying them in a large, diverted tokamak. A recent campaign on JET has therefore sought to address some of the important questions related to helium operation (He concentrations near 90%) in single null configuruations, particularly with regard to edge and divertor physics. This contribution compiles a selection of results from these experiments, in which, in each case, discharges have been chosen to match as closely as possible previous, well characterised D plasmas in both L and ELMing H-modes. These matched pulses are used to draw conclusions regarding the princple source and location of carbon production in D plasmas, to compare and contrast the mechanisms of the density limit and the detachment process in D and He, to investigate the nature of cross-field power transport in the SOL and to gain insight into the process by which ELM energy is transported to the divertor targets.

1. INTRODUCTION

Operation in helium is considered as one option for the low activation phase of ITER. To date, however, with the exception of a short campaign on the DIII-D facility [1], pure helium plasmas have constituted a negligible fraction of discharges executed in large diverted tokamaks. In a graphite containing machine (as presently forseen for ITER [2]), the absence of carbon chemistry in a pure He plasma is expected to significantly modify the source of impurity production. The recycling nature of He compared with D and the significant differences in He atomic physics might be expected to strongly influence global particle balance, SOL transport, divertor physics, density limits and perhaps ELM transport in the edge plasma. With these key issues in mind, together with the important apsects related to the L-H transition threshold and energy confinement, an extended series of pure He experiments has recently been performed on JET. This contribution compiles some of the more important edge and divertor physics observations resulting from this campaign. Companion papers providing more detail may be found within these proceedings and are appropriately referenced in the text.

2. EXPERIMENT AND DIAGNOSTICS

A total of over 100 JET pure He discharges have been dedicated to the study of edge physics issues, following a programme closely matching previous pulses in D for comparative purposes. A large majority of experiments are conducted in one of two single null lower equilibria with high or low wall clearance (Fig.1) frequently used at JET (all with the $B \times \nabla B$ drift direction towards the X-point). All have been performed in the Mark IIGB divertor configuration with wall temperature at $200^{o}C$ (some comparison D pulses were at higher $T_{wall} = 320^{o}C$). Divertor targets are in graphite, in common with poloidal armour on the central column. The possibility at JET for conversion of the D neutral beam injection (NBI) sources to He^{4} has allowed both L-mode and ELMing H-mode plasmas to be compared with P_{NBI} available up to 12MW. With the exception of a handful of very

high power discharges, NBI was the sole additional heating source used in these experiments. Argon frosting on the NBI cryopanels was required between He pulses for reliable beam operation, but the use of helium as working gas precluded efficient divertor cryopumping (unlike in companion D pulses). An early important result from these He discharges was the discovery of an L-H transition threshold power ~50% higher in He than D and an energy confinement in H-mode ~0.83 that of an equivalent D discharge [3]. The lower NBI power available with pure He beams, the lack of density control and the higher H-mode threshold prevented Type I ELMing H-mode He pulses at I_p,B_T combinations typical of D discharges (2.5MA, 2.5T).

Essential visible spectroscopic diagnostics from the point of view of this paper are wide-angle views of the inner and outer divertor regions looking from the top of the machine and a horizontal Line-Of-Sight (LOS) viewing the inner wall at the plasma midplane (recycling fluxes, intensity of CIII line emission). In addition to the standard foil bolometry, data from tangentially viewing divertor CCD cameras equipped with interference filters (D_α, HeI, HeII) and a poloidally scanning VUV spectrometer are also available. Target Langmuir probes, IR thermography and tile embedded thermocouples provide divertor plate parameters, with a reciprocating Langmuir probe and lithium beam used to obtain profiles in the main SOL plasma. Total pressures in the subdivertor and main chamber are monitored using penning gauges.

3. D-He CHANGEOVER

The switch from D to He and back was performed in a low clearance discharge using ICRH power ramps to monitor the development of the L-H transition threshold as the working gas was exchanged. Helium concentrations, monitored both by the ratios of He and D_2 partial pressures in the subdivertor (accounting for the enhanced cryopumping of D_2) and edge spectroscopy, show the ratio He/(D+He) reaching 80-85% during in the ohmic phase of the first changeover discharge, decreasing later to ~50% with ~7.0 MW of ICRH [4]. The effect of heating on the ratio was reduced to negligible levels after 8-9 repeated discharges. Throughout the campaign, the ratio was typically in the range ~90-95%.

4. IMPURITY PRODUCTION

4.1. GENERAL OBSERVATIONS

Emission from the molecular species CD and C_2 in the outer divertor fell to undetectable levels after just the first two He fuelled discharges of the changeover. In the inner divertor, a large decrease in the first discharge was followed by a slower decrease with further pulses, attributed to erosion of saturated C films providing a hydrocarbon source (the inner divertor in JET is known to be colder and more dense, detached at anything but low density and a region of net redeposition in D, the outer an area of net erosion [5]). Operation in pure helium helps to illustrate this further using the response of the target surface temperature, T_{surf}, to NBI power steps, examples of which, for matched D and He discharges are compared in Fig.2. Measured using IR thermography, at the outer target in

D plasmas, $T_{surf} \propto \sqrt{t}$ in response to each power step as expected. Such behaviour is not observed at the inner target in D, where the response more closely matches the power staircase waveform. Moreover, tile calorimetry shows conclusively that most of the power is deposited in the outer divertor, even though $T_{surf}^{inner} > T_{surf}^{outer}$ from thermography. In He plasmas, $T_{surf} \propto \sqrt{t}$ at both targets and $T_{surf}^{inner} > T_{surf}^{outer}$, in accordance with calorimetric power balance. The different temperature responses to incident power for D compared to He is an indication of a surface modification during D operation. This modification can be modelled as a reduced thermal conductivity at the surface and is thought to be due to redeposited material. A detailed interpretation of the IR measurements is the subject of a companion paper [6].

Conclusions regarding the general behaviour of C sources in JET can be drawn by comparison of matched D and He discharges, one L-mode example of which is shown in Fig.3. These are two low clearance equilibria for which, during the period of NBI heating, the total input power (Fig.3(b)) is similar in both He and D, albeit it for a 20% higher D plasma density (Fig.3(a)). This is due to a strong D_2 puff into the outer divertor during this time for the D discharge (Fig.3(j) - a second D_2 puff follows later into the inner divertor). The incremental Z_{eff} (Z_{eff} - 1 for D and Z_{eff} - 2 for He) in Fig.3(d) demonstrate the cleanliness with respect to core carbon content of these He discharges (XUV and VUV core spectroscopy show the light impurities C and O to be reduced generally by about a factor 10 in L-mode He plasmas). This is correlated with a reduction of a factor 3 in the intensity of inner midplane CIII (465 nm) emission (Fig.3(e)) whilst inner and outer divertor CIII signals are of similar magnitude in D and He during the beam heating phase for this pair of discharges (Fig.3.(f,g)).

The midplane and subdivertor pressures in Fig.3(h,i) vary strongly in the D plasma owing to the intense gas puffs, but at ~19.8s into each discharge (marked by the dashed line), there is a point where $\bar{n}_e$ in both cases is identical. Although this is not a steady state situation,at this time outer midplane pressures are approximately equal in He and D,whilst the ratio of D and He subdivertor pressures is ~6. Such a large difference in compression ratios would appear to rule out the existence of strong bypass leaks from divertor to main chamber in JET. Since the penning gauge is sensitive primarily to molecules in D and atoms in He, for similar pressure in He and D, one expects the original neutral flux to have been a factor 2 higher in D.

At t = 18s in each of these discharges, Fig.4 compares SOL profiles, mapped to the outer midplane, of n_e,T_e and parallel flow Mach No., combining data from a reciprocating Langmuir Some edge LIDAR data are also in included. The similarity between D and He profiles is remarkable, with differences between the diagnostic signals for the same discharge easily accounted for within the alignment precision of the various systems The high values of parallel flow (Fig.4(c))seen in D for forward field direction are apparently present also in He plasmas, as is the peaked structure often seen in D plasmas [7]. Fig.5 compares a further two pairs of illustrative matched high clearance discharges, the first for an L-mode density ramp (density limits will be discussed further in Section 5 - see Fig.7 for another pair of matched density limit pulses, this time in a low clearance

configuration) and the second for a pair of Type I ELMing H-mode discharges at low Ip and BT (1.0MA/1.0T). In comparison with the "larger" equilibria (Fig.1(a)), higher wall clearance in L-mode leads to still lower main chamber and inner divertor carbon levels (more than a further factor of 2 lower) than in equivalent D discharges. At low to medium $\bar{n}_e$,the outer divertor carbon emission is again comparable in He and D,but with rising density, carbon emission in the He plasma falls to undetectable levels everywhere. Before the onset of divertor detachment (section 5), at the same value of $\bar{n}_e$,subdivertor and midplane pressures behave similarly to those in the shot pair of Fig. 3.In the Type I ELMing H-mode (RHS of Fig.5),CIII intensities are comparable at all locations in both D and He and midplane pressures are again similar (though these are averaged values over the ELMs).

4.2. DISCUSSION

Qualitatively, the observations described above for L-mode diverted plasmas are consistent with a picture in which carbon chemical sputtering accounts for a large fraction of the impurity source in D plasmas, particularly at medium to high densities. Quantitative conclusions regarding the regional (inner/outer divertor, main chamber walls) dependence of the source strength are more problematic, due principally to the difficulty in deriving absolute fluxes from the spectrosopic lines of sight (LOS), particularly in the divertor, where strong (unmeasured) variations in the local n_e and T_e translate to considerable variations in the photon efficiencies (S/XB) and hence in the derived carbon source rates. The fact that in He at high density, CIII emission decreases to low values everywhere, whilst in D it remains constant or even increases in the main chamber (as evident in the density limit discharges of Figs.5,7), points strongly to a chemically sputtered source, since ion energies at the target plates under these conditions are below the threshold for physical sputtering (in D and He) even at the hotter, more attached outer target.

In the absence of more extensive diagnostic coverage, code simulations offer the only real chance of quantifying both the source strength at any particular location and its efficiency in contaminating the discharge (screening). Such simulations are now in progress for these helium plasmas, using both the two edge codes currently in use at JET, the EDGE2D-Nimbus and SOLPS5 (B2.5-Eirene) packages and the US fluid plasma code UEDGE. The latter has been applied in particular to examine the differences in divertor carbon source rates in D and He by obtaining the best match to experimental target and upstream plasma conditions and then computing averaged S/XB's along the LOS of a poloidally scanning VUV spectrometer observing CIV emission at 31.2 nm and a CCD camera measuring the intensity of the CII visible line at 658 nm. Both are vertically viewing and both offer good poloidal coverage of the divertor region.

For matched high clearance baseline reference L-mode cases with $n_e = 3.6 \times 10^{19}$ m^{-3} and I_p =2.4 MA, B_T =2.4 T and P_{NBI} ~3MW,comparison of experiment and code indicate that in the He pulse there is reduction in the inner divertor C^+ source by a factor 4,a reduction of the C^{3+} source by a factor of 12 throughout the divertor and a comparable C +source at the outer target in both D and

He.This comparison suggests that the outer divertor C source is not a major factor in determining that of the higher ionisation states which eventually lead to core contamination.Similar analysis for higher power or density shows that the dominant source for divertor C production in He is ion physical sputtering,that the latter is also present in D at the attached outer target (but perhaps does not contribute significantly to core contamination)and that chemical sputtering at the inner divertor is a major contributor.A detailed discussion of the results can be found in a separate paper to these proceedings [8].

Concerning main chamber sources, some preliminary B2.5-Eirene results compiled in Fig.6 concerning the poloidal distribution of ion (D^+ and He^{2+}) and neutral (D_0 and He_0) perpendicular outfluxes are of interest. Dividing the ordinate by the electronic charge gives a number of particles in each of 96 equal angle bins covering the 360^o of one poloidal section. The data are generated from a standalone Eirene run based on a converged SOLPS5.0 plasma solution and have not yet been converted to fluxes at the wall surfaces. Particle balance has been verified so that neutral influx to the code is balanced by the sum of the ion and neutral outfluxes presented in Fig.6. The simulations are appropriate to the low clearance discharges of Fig.3, albeit at code separatrix density of $n_{e,sep} = 8 \times 10^{18}$ m^{-3}, about a factor of two higher than indicated in the experimental profile data of Fig.4.

Ion outfluxes in the main chamber behave as expected, with $\Gamma^{He2+} \sim 0.5\ \Gamma^{D+}$ and are comparable to the neutral outfluxes everywhere except at the inner midplane location, where Γ^{D^0}, is more than a factor 100 greater than any other ion or neutral loss. Elsewhere, $\Gamma^{D^0} \approx 3.5\ \Gamma^{He^0}$, consistent with reduced charge exchange reaction rates in He compared with D at the energies characteristic of the SOL. This accumulation of neutrals in D at the inner wall, due probably to leakage from the colder, more dense inner divertor, would appear to explain why midplane horizontal spectroscopic ionisation fluxes (from HeI and D_α emission) in the discharge pair of Fig.3 differ by a factor of ~50 (even in the absence of strong gas puffing in D), whilst the outer midplane penning gauge pressures in He and D are similar - the horizontal spectroscopic LOS is dominated in D by emission from the inner wall. Indeed, by normalising to these line emission fluxes, the FRANTIC code [9], which numerically solves the 1D time-independent kinetic equation describing the neutral density distribution using experimental n_e and T_e (Fig.4) profiles, yields He^0 and D^0 densities consistent with the simulation results of Fig.6. In doing so, the code assumes neutral birth energies of ~4eV (D) and ~20eV (He), derived from Doppler broadening of D_α and HeII lines [10], consistent with molecular dissocation (D) and ion reflection (He) being the main wall recycling source.

Taken together, these results imply that in He L-mode, ion sputtering at the main chamber walls (particularly the inner wall which represents the largest graphite surface area) is the principle source of main chamber carbon production. This is further supported by the observation (see above) of still further reduced CIII emission (compard with D) in the inner divertor and at the midplane in moving from low to high wall clearance - the reduced plasma-wall distance likely increases the He ion physical sputtering source of carbon near the inside top of the vacuum vessel (Fig.1). In D,

since chemical sputtering yields at the fluxes and energies characteristic of the far SOL exceed the maximum of the D physical sputtering yield [11] carbon chemical sputtering by neutrals almost certainly dominates the source, particularly at high density where main chamber C emission is observed to increase in D (Figs.5,7) and ion energies at the wall are likely below the threshold for physical sputtering.

5. DETACHMENT AND DENSITY LIMITS

Just as the absence of carbon chemistry in He discharges can be used to imply chemical sputtering as the main source of impurity production in L-mode D plasmas (section 4), the differing atomic physics and recycling properties of He and D may be invoked as the principal factors in explaining the higher density limit observed in He compared with equivalent D discharges. The details are presented in an accompanying paper [12], where it is demonstrated that the enhanced density limit in He (up to a factor 2.8 higher than in D depending on wall clearance), is a consequence of reduced ionisation rate coefficients (longer mean-free paths for He neutrals in the cold divertor plasma at high density), higher He^0 energy in comparison with D^0 (section 4) and significantly lower charge exchange and elastic collision rates in He. This combination leads to an increased neutral penetration depth (enhanced neutral leakage from the divertor) such that, although an X-point MARFE forms at similar densities in both D and He, in the He plasma the density can be increased continuously until the radiative power fraction reaches 100%. In deuterium, increasing density beyond the X-point MARFE leads to the formation of an inner wall MARFE and a rapid (in density) approach to 100% radiation [13]. Also important is the increased efficiency of ohmic heating in He ($P_\Omega \propto Z_{eff}$), leading to higher heating powers (for the same Ip) and hence a higher achievable density before radiative collapse.

In H-mode, it appears that the D and He density limits (defined as the density at the H-L-mode back-transition) are very similar [12]. It is arguable, however, that the increased L-H transition threshold and significantly different recycling properties of He make comparison with equivalent D pulses somewhat unfair.

The increased He neutral penetration in comparison with D also produces significant differences in the divertor detachment behaviour of He plasmas. Detachment in D is well documented in JET [14] and elsewhere [15] and is compared with the observations in He in Fig.7. Both the density and radiated power fraction (Fig.7 (a,b)) are well matched temporally in these two high clearance discharges - the higher density limit in He is evident (as it was in Fig.5 for the high clearance L-mode density limit discharges #53080 and #54030). The CIII signals (Fig.7 (d-f)) indicate the same trends as discussed in Section 4: rising with in the main chamber in the D pulse, becoming negligible in He, reaching constant values in the divertor at high density in D and falling to zero in He. Subject to the uncertainty in interpretation due to changing photon efficiencies, these observations indicate a strong role for carbon chemical sputtering in the divertor D with increasing $\bar{n}_e$. This conclusion is supported by the strike point T_e measurements in Fig.7(i), in which, for the inner target, T_e is too

low (< 10eV) in both D and He for physical sputtering to be a serious contributor to the observed C source. At the outer target, T_e is high enough for the yield due to physical sputtering to contribute significantly to carbon production in both He and D at low densities, but cannot at higher $\bar{n}_e$, resulting in the gradual decrease of the CIII intensity to low levels in He. The divertor source remaining at high density in D must therefore be attribruted practically solely to chemical sputtering.

In Fig.7(g), the wide angle D_α emission from the inner divertor rises rapidly with despite the decreasing integrated ion flux to the target plates (Fig.7(h)) - the classic signature of total detachment at the inner target [14]. In contrast, the outer target ion flux in D rises with density, as does the D_α emission, indicating that the attached, high recycling state is maintained in the hotter outer divertor (Fig.7(i)) right up to the density limit. In He, detachment begins at much higher upstream densities and is similar to that in D only in the sense that the inner target appears to detach first. What is different is the decrease in power flux, especially at the inner target, (Fig.7(j), measured by IR thermography), long before the particle flux.

Although Figs.7(h,j) compare a peak power flux with an integrated target ion flux, the same is also true at the strike point - the ion flux detaches long after the power flux. Such behaviour was also observed during similar experiments on DIII-D [16] and is in contrast to the general picture in D whereby ion-neutral frictional processes [15] at low divertor T_e and eventually recombination [17] reduce the target ion flux. In He, the increased increased mean-free-path for neutral ionisation allows He neutrals to progressively escape the divertor volume to regions beyond the X-point, where intense line radiation (mostly from He_+), leads to a pressure collapse in the SOL plasma. Increasing the power into the same discharge can prevent particle detachment in both inner and outer divertors right up to the density limit.

The rapid movement and spatial localisation of the radiation front with increasing $\bar{n}_e$.in the colder inner divertor are reflected respectively in the HeI line intensity of Fig7.(g) and the bolometric inversions of Fig.8(b), which should be contrasted with the distribution of radiation in the D case (Fig.8(a)). Similar trends are also seen in the reconstructed emission from 2D tangential CCD camera observations of the divertor and X-point HeI,II line emission. Equally, the plateau value of midplane pressure and collapse in the subdivertor pressure in He as the radiation moves to the X-point should be compared with the monotonic increase of both up to the density limit in D (Fig.7(k)). One may also note that to obtain consistency in the reconstruction of the total radiation using in-divertor and ex-divertor bolometer lines of sight [18], a neutral contribution of up to 20% of the power measured by divertor bolometers must assumed for D plasmas, whilst no such contribution is required for equivalent He discharges.

Most of these experimentally observed features can be reproduced by simulations, first performed for DIII-D with the B2-Eirene code by Loarte [19]. For JET, modelling has been performed with both the EDGE2D-Nimbus package and with the B2.5-Eirene code, with results from the latter being presented in a companion paper [20].

6. L AND H-MODE SCRAPE-OFF LAYER TRANSPORT

The technique of divertor target strike point sweeping across tile mounted Langmuir probes and embedded thermocouples to obtain peak parallel field power flux densities and deposited power profiles (from which power scrape-off widths, λ_q can be derived) in both L and ELMing H-mode D discharges has been pioneered at JET and is well documented in the literature [21,22]. In the absence of strong D_2 puffing and under high power conditions, a narrow feature appears in the power profile which is being interpreted as due to inter-ELM ion orbit losses from the pedestal region. More details of the complex numerical modelling demonstrating this phenomena can be found in a separate contribition to these proceedings [23].

During the He campaign a series of strike point swept, high clearance pulses have permitted a number of additions to the D database, notably the inclusion of a previously unavailable A(Z) dependence and some parameter variation in q_{95} and B_T. Unfortunately, the lower NBI powers available and the increased (compared to D) L-H transition power, restricts the new He data to Type III ELMing H-modes at lower I_p /B_T combinations, typically 1.5MA/1.5T, in comparison with the standard combination for shots populating the D database (2.5MA/2.4T). Figure 9 compiles a selection of the D and He data (restricted for clarity to constant $q_{95} = 2.6$) for the variation with P_{SOL} of λ_q and λ_q at the outer target (where most of P_{SOL} is deposited in both D and He (see Fig.2)). Data points denoted by the label TC are obtained from thermocouple analysis, representing the total (ion and electron) deposited power, whilst LP refers to the result of applying standard sheath theory to compute the parallel (electron) power flux from target probe measurements of T_e and particle flux.

As described elsewhere [22], the D points demonstrate clearly that in high power H-modes, ions dominate the energy balance (q(TC) >> q(LP)). For He, there appears to be a much stronger coupling between ions and electrons up to the maximum P_{SOL} achievable in these experiments. This could be due both to the increased ion-electron collisionality in He and a lower fraction of hot ions (due to lower pedestal temperatures in the He Type III ELMing H-modes). In general, there is tendency for $\lambda_q^{He} > \lambda_q^{D}$, particularly in H-mode. Regression analysis performed on the TC l_q data [24] with respect to the variables Z, B_T,P_{SOL} and $n_{e,sep}$ yields: $\lambda_q \sim Z^{0.92}\ B_T^{-1.03}\ P_{SOL}\ n_e^{-0.14}$, showing a strong charge and magnetic field scaling, a weak density dependence and preserving the negative power exponent previously derived in analysing D data alone [22]. Assuming that ion convection dominates the parallel mass transport, this parametric dependence, when compared with a large number of candidate models describing cross-field energy transport is closest to that which would be expected on the basis of a classical scaling for $\chi_\perp$.

6.1. ELM DURATIONS

Although the Type I ELMing H-mode regime is foreseen as the reference scenario for inductive operation of ITER [2], the large divertor target power loads and intolerable erosion that can result when extrapolations are made to next step devices is a cause for serious concern. Understanding the mechanism by which the heat and particles expelled by the ELM arrive at the target plates is

thus of great importance. Previous analysis of the ELM power pulse duration using IR thermography on the JET and ASDEX-U divertor targets indicated a correlation of this time with the parallel loss time for ions to flow from the upstream (outer midplane) location of the ELM event along field lines to the divertor [25]. This characteristic time was taken as $\tau_{\|} = 2\pi Rq_{95}/c_s(1+\sqrt{3}/2\nu^*)$ with c_s the sound speed (evaluated for T_i and T_e) at the top of the pedestal and $\nu^* = 2\pi Rq_{95}/\lambda$ with λ the mean-free-path for ion-ion collisions. New data from the JET pure helium experiments indicate that the key element determining the transmission of energy to the targets is simply the arrival time of the ion pressure wave front, given by $\tau_{\|} = 2\pi Rq_{95}/c_s$. This is shown in Fig. 10, where, τ_{IR}, defined as the rise time of T_{surf} due to the ELM, is plotted as a function of $\tau_{\|}$ from JET and ASDEX-U deuterium Type I ELMing H-modes and in which two new JET He points have been added [26]. These τ_{IR} helium points are from discharges with an I_p,B_T combination of 2MA, 2T, somewhat lower than the values typical of the JET deuterium H-modes and represent an average over just a handful of Type I ELMs obtained immediately after the L-H transition with ~12MW of He NBI power before a transition to Type III ELMs. On the basis of Fig.10, the ELM power duration on ITER ($\tau_{\|} \sim 220\mu s$), would be expected to be in the range ~500μs.

CONCLUSIONS

A recent JET campaign of pure He plasmas with He neutral beam injection has provided a wealth of data which, in addition to providing valuable information with which to judge the merits of He as an option for fueling the discharges of the ITER low activation phase, offer interesting new insights into D operation. The combinination of spectroscopic observations from and code simulations of these plasmas indicates strongly that carbon contamination of the discharge in L-mode D plasmas in JET is dominated by chemical sputtering (due to ionic and neutral fluxes) at the inner wall and at the inner divertor. In He, where carbon chemistry is absent, ion physical sputtering dominates, but is at such a low level compared with the combination of chemical and physical processes in D that Z_{eff} in L-mode diverted discharges is close to that expected in a pure He plasma.

Divertor detachment is very different in He, being driven by the escape of recycling neutrals from the divertor volume to the X-point region where the resulting intense radiation from ionisation of He neutrals and He^+ ions starves the divertor of power and leads, eventually to particle flux detachment. This, together with the lower charge exchange rates in He, is the principle reason for L-mode density limits a factor of 2-3 higher in He compared with equivalent D plasmas. The increased atomic number in He permits the addition of a further parameter in the regression analysis of SOL power scrape-off widths, already the subject of detailed study at JET in D plasmas. First results indicate that classical cross-field transport comes closest to describing the radial heat flux in the JET scrape-off layer. Although data are sparse, results from these He plasmas point strongly to the validity of a picture in which the ELM energy released in the main SOL propagates parallel to the field lines down to the divertor targets with speed governed only by that of an ion pressure wave travelling at sonic speed appropriate to the upstream pedestal T_e, T_i.

In He the L-H transition power threshold is found to be higher than in D by about a factor 1.5, with energy confinement ~75% of that in D. For the ITER low activation phase, helium is therefore preferable to hydrogen from the point of view of threshold power (at the expense of confinement), but the JET results presented here indicate that He operation would not provide an adequate test of critical divertor physics issues for the next step. In particular, if ITER is to employ graphite armour in the divertor during the early phase of operation, He plasmas would not provide an adequate comparative (to D) test of target erosion (and fuel retention).

Likewise, divertor detachment and pumping in He are so different that a campaign in hydrogen would appear to be more attractive with respect preparing for the later D-T operation phase.

ACKNOWLEDGEMENTS

This work was performed under the European Fusion Development Agreement and was supported in part by the Swiss National Science Foundation, EURATOM and the UK, Department of Trade and Industry.

REFERENCES

[1]. W. P. West et al., J. Nucl. Mater **266-269** (1999) 732
[2]. Nuclear Fusion **39** (1999) 2137
[3]. D. McDonald et al., Bulletin Am. Phys. Soc., Vol ? (2001), Paper QO1.002
[4]. D. Hillis et al., these proceedings (PSI-15)
[5]. J. P. Coad et al., J. Nucl. Mater **290-293** (2001) 224
[6]. P. Andrew et al., these proceedings (PSI-15)
[7]. S. K. Erents et al, A. V. Chankin, G. F. Matthews and P. C. Stangeby, Plasma Phys. Contr. Fusion **42** (2000) 905
[8]. M. E. Fenstermacher, G. Porter et al., these proceedings (PSI-15)
[9]. S. Tamor, SAI Report 023-79-1056LJ
[10]. Ph. Mertens et al. Plasma Phys. Contr. Fusion **43** (2001) A349
[11]. V. Philipps et al., these proceedings (PSI-15)
[12]. J. Rapp et al., these proceedings (PSI-15)
[13]. J. Rapp et al., Proc. 28th EPS Conference on Contr. Fusion and Plasma Phys., Funchal, 18-22 June 2001, ECA Vol. **25A** (2001) 981
[14]. A. Loarte et al, Nucl. Fusion **38** (1998) 331
[15]. C. S. Pitcher and P. C. Stangeby, Plasma Phys. Contr. Fusion **39** (1997) 779
[16]. D. N. Hill et al., 13th International Conf. on Plasma-Surface Interactions in Contr. Fusion Devices, San Diego, CA, USA, May 18-22, 1998, unpublished.
[17]. G. M. McCracken et al, J. Nucl. Mater **266-269** (1999) 37
[18]. L. C. Ingesson et al., Proc. 26th EPS Conference on Contr. Fusion and Plasma Phys., Maastricht, 14-18 June 1999, ECA Vol. **23J** (1999) 257

[19]. A. Loarte et al., Contrib. Plasma Phys. **40** (2000) 3
[20]. M. Wischmeier et al., these proceedings (PSI-15)
[21]. V. Riccardo et al., Plasma Phys. Contr. Fusion **43** (2001) 1
[22]. W. Fundamenski et al., Plasma Phys. Contr. Fusion **44** (2002) 1
[23]. W. Fundamenski et al., these proceedings (PSI-15)
[24]. W. Fundamenski, in preparation
[25]. A. Loarte et al., submitted to Plasma Phys. Contr. Fusion.
[26]. T. Eich et al., these proceedings (PSI-15)

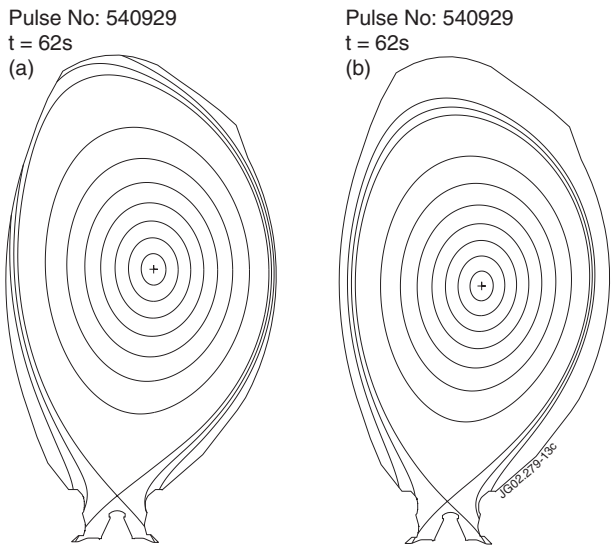

Figure 1: low (a) and high (b) wall clearance equilibria used for the majority experiments described in this paper.

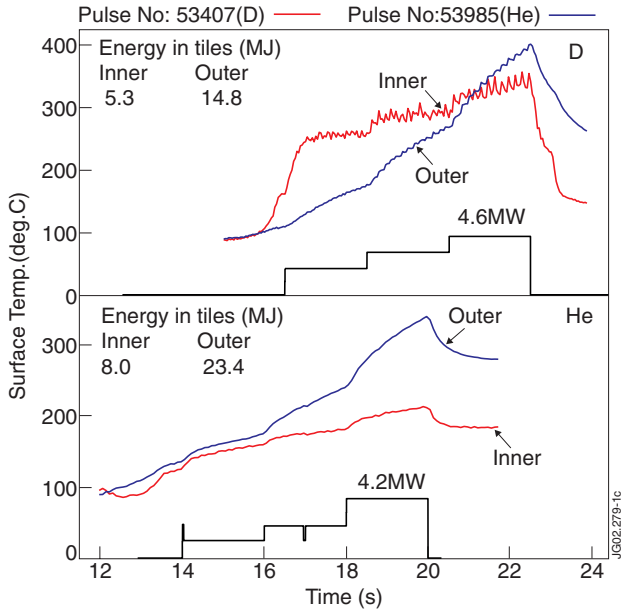

Figure 2: Response of peak surface temperature on inner and outer divertor targets to NBI power steps during D (#53407) and He (#53985) plasmas. The discharges are matched, L-mode, high wall clearance discharges with I_p = 2.4MA, B_T = 2.4T. The total energy deposited on the inner and outer divertor vertical tiles at the end of the shot from thermoucouple analysis is also given.

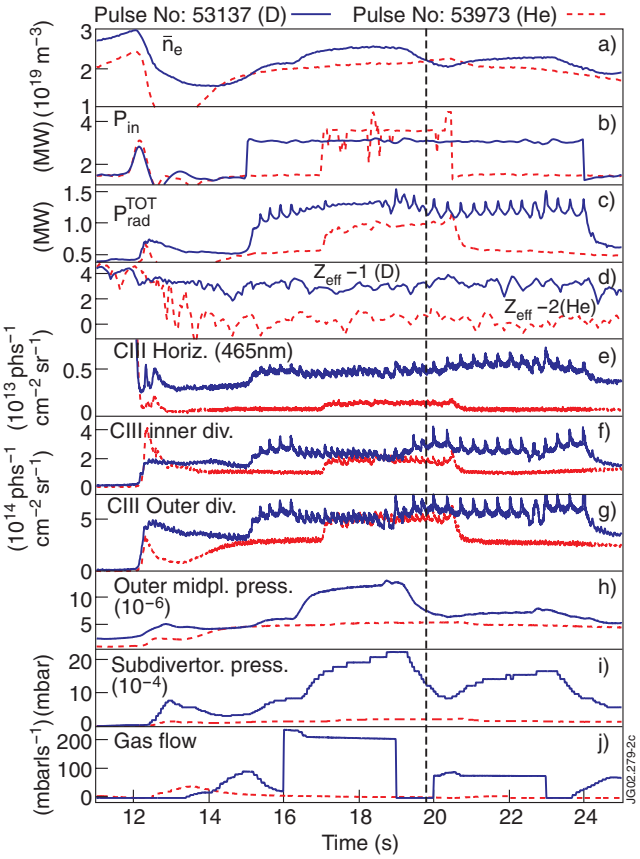

Figure 3: Comparison of matched L-mode D and He shots at I_p = 2.4MA, B_T = 2.5T: full blue lines D (#53137), dashed red lines He (#53973). These are low wall clearance discharges. The dashed vertical line at 19.8s shows how when the plasma density is very similar and the D gas fuelling is low, midplane pressures are almost the same but subdivertor pressures are about a factor 6 lower in He compared with D.

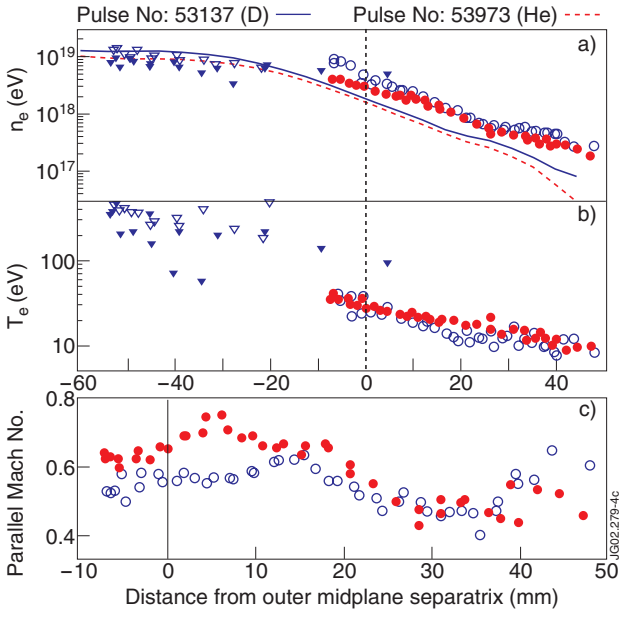

Figure 4: Comparison of edge n_e,T_e (a,b) and Mach No. profiles (c) at t = 18s for the matched He and D shots in Fig. 1 showing the remarkably similar edge conditions for two very different plasma species. Open symbols (D), closed symbols (He), circles (RCP), triangles (Edge LIDAR), lines (Li beam): full (D), dashed (He). The slightly higher density in the D case is due to the higher (Fig.2(a))at the chosen measurement time.

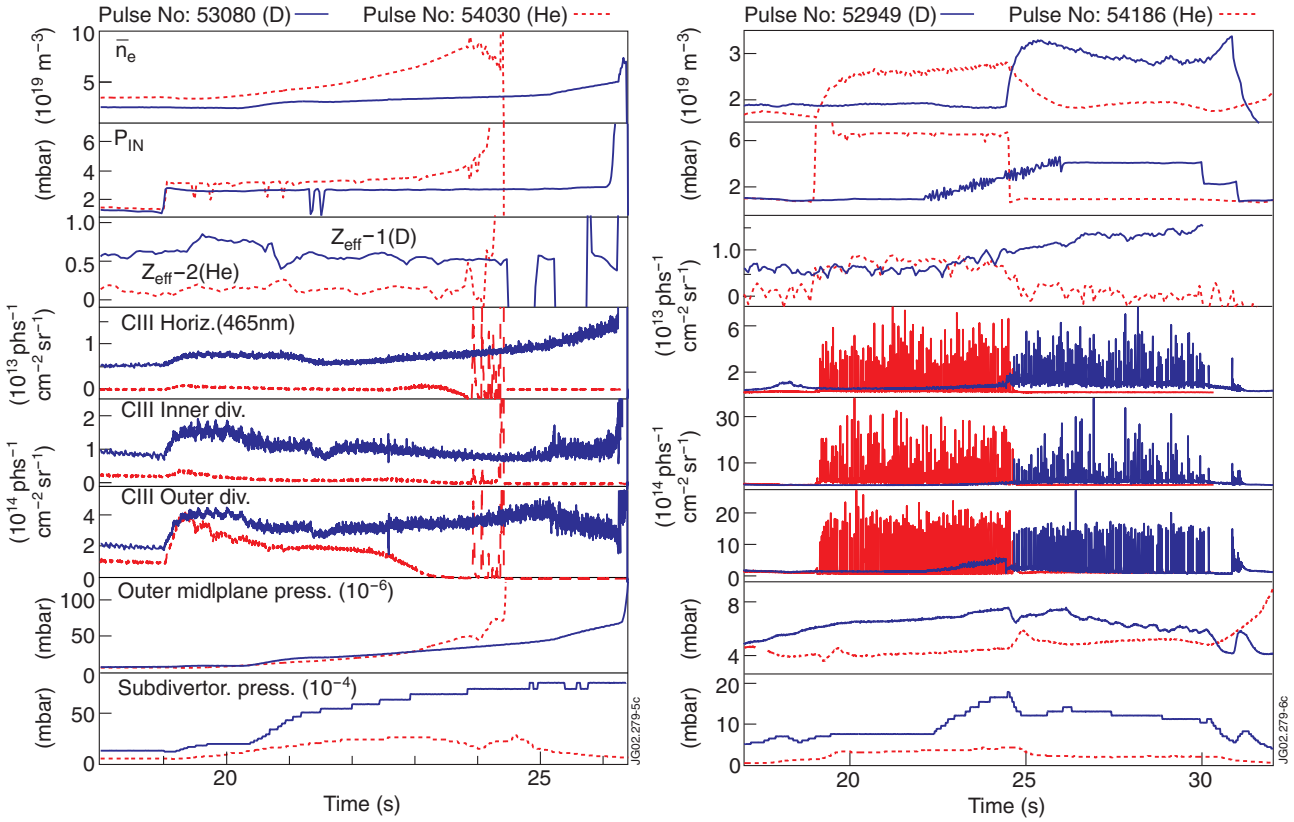

Figure 5: Comparison of matched L-mode D and He density limit shots at I_p = 2.4MA, B_T = 2.5T (left) and matched low clearance Type I ELMing H-mode discharges at I_p = 1.0MA, B_T = 1.0 T (right). Full blue lines D, dashed red lines He. Both shot pairs are low wall clearance discharges. In the density limit discharges, gas puffing is in both cases into the outer divertor.

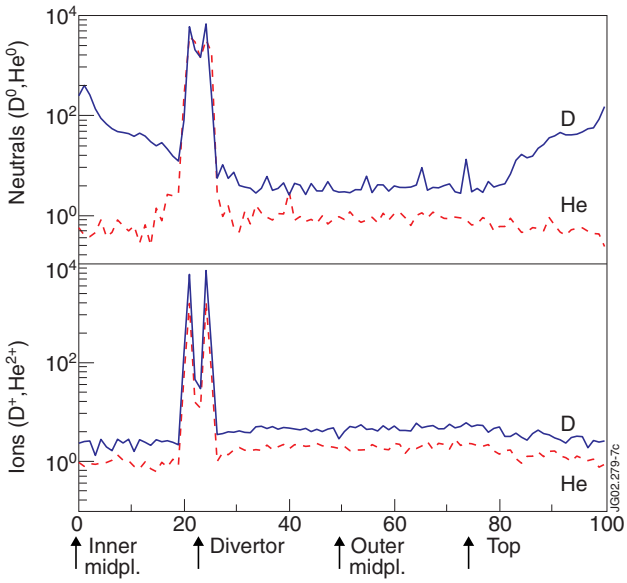

Figure 6: Simulated poloidal distributions of neutral and ion outfluxes for D (blue lines) and He (red dashed lines) from SOLPS5 on a low clearance equilibrium with $n_{e,sep} = 10^{18}$ m^{-3} , P_{SOL} ~ 3MW and , $D_\perp = 0.2$ m^2 s^{-1},$\chi_\perp = 1.0$m^2 s^{-1}. The dominant contribution from the divertor is evident in both ion and neutral outfluxes.

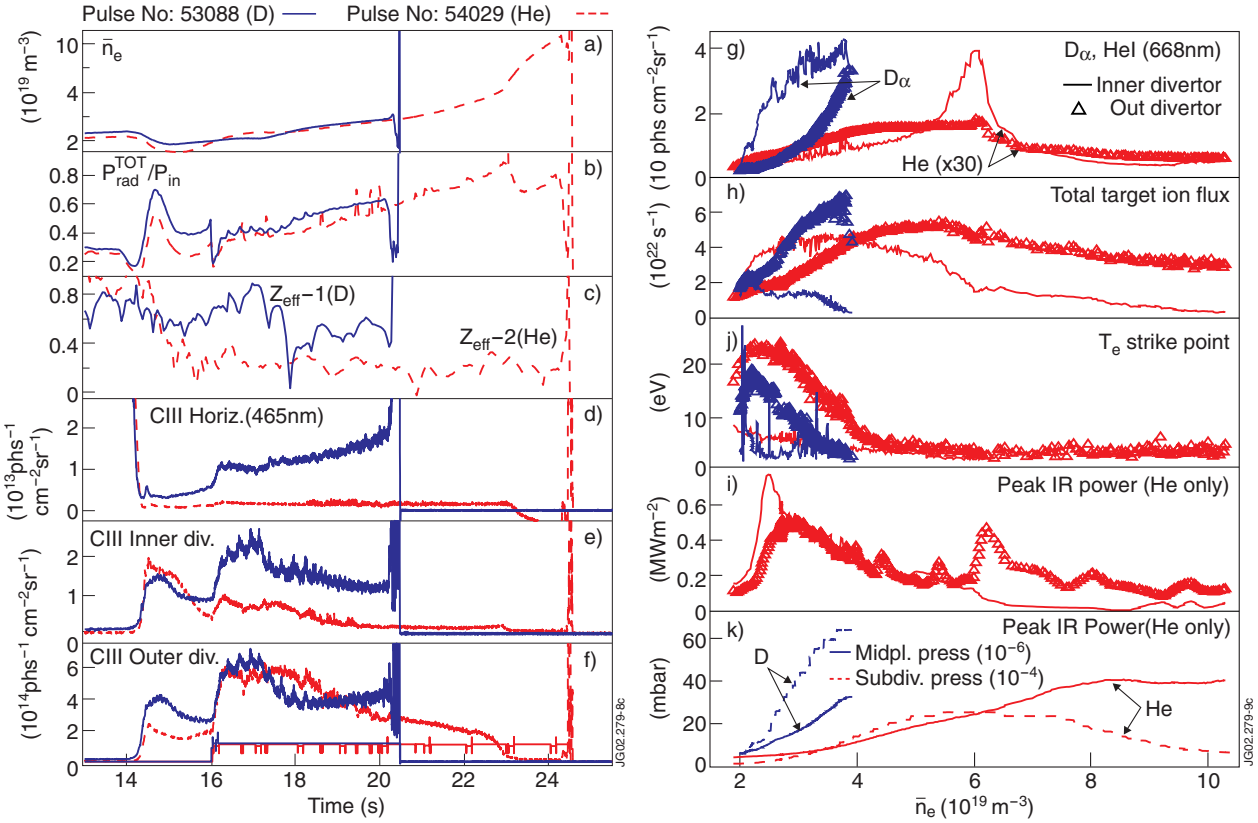

Figure 7: Comparison of matched D (blue) and He (red) density limit discharges at I_p = 2.0 MA, B_T = 2.4T. The configuration has low wall clearance, as in the matched pair of Fig.1. Note that IR data are available only for the He discharge. The step in CIII fluxes at 16s indicates the switch-on of ~1.1MW of NBI power which is maintained in each case until disruption. Note that the plots on the RHS are given as a function of density and that the symbols represent outer target quantities and the full lines the inner target in each case.

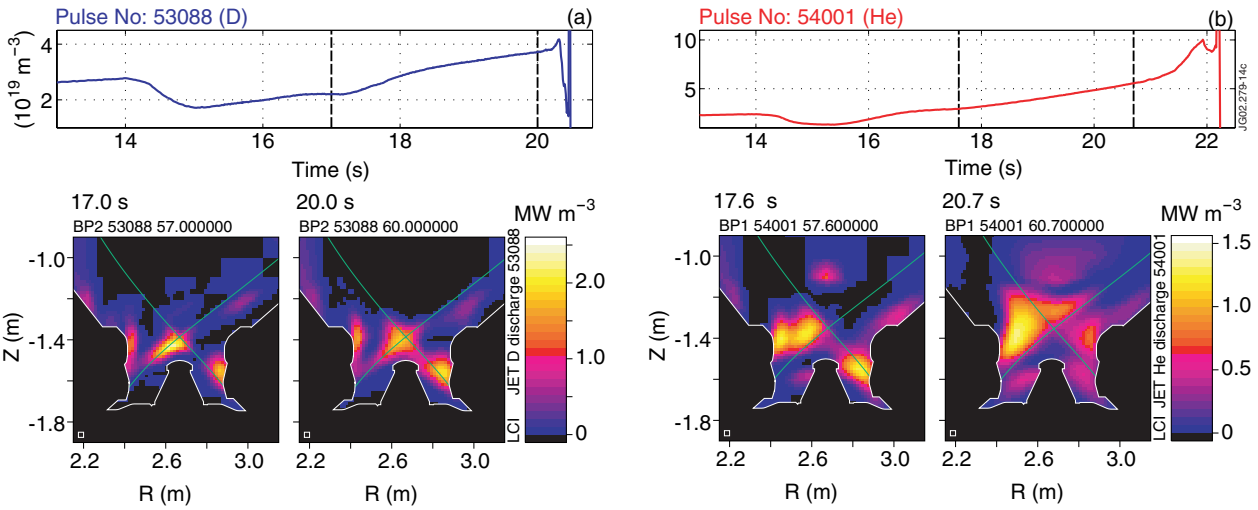

Figure 8: Illustrating the differences in divertor total radiation distributions in the nearly matched shot pair (a) #53088 (D) and (b) #54001 (He). The vertical dashed lines in the time traces of density indicate the times at which the bolometric inversions have been performed. Note that in both cases, the reconstructions correspond to plasma densities below the onset of the inner wall MARFE in D and the fully developed X-point MARFE in He [12].

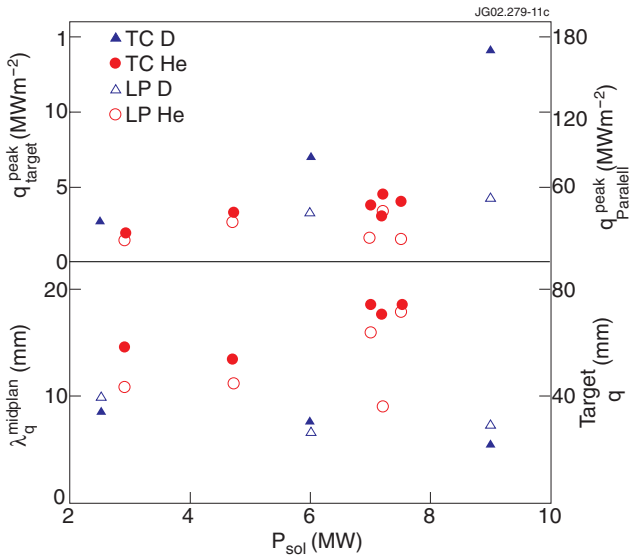

Figure 9: Dependence of peak target heat fluxes and midplane power scrape-off lengths at the outer as a function of power reaching the SOL for heated L and H-mode D and He plasmas in high clearance equilibria. Whilst the points to varying I_p and B_T, q_{95} = 2.6 in all cases. and TC refer to quantities measured with divertor probes and tile thermocouples respectively.

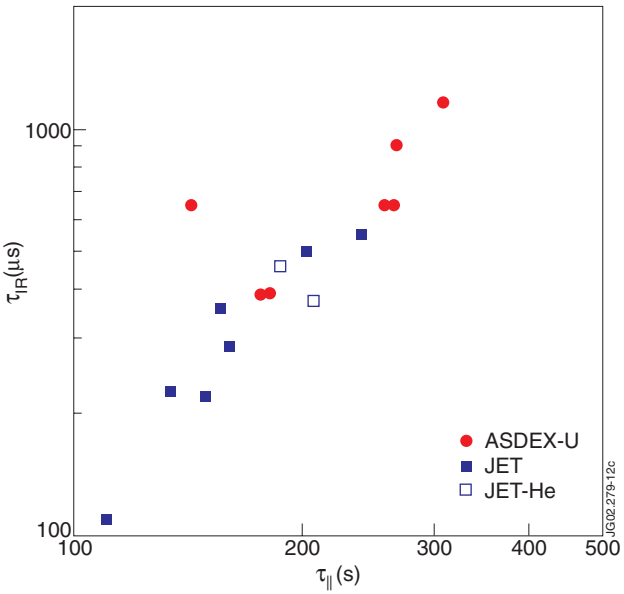

Figure 10: The variation of ELM target power times measured by thermography with for parallel propagation of the SOL pressure travelling at sound speed from the upstream of the ELM event to the outer targets in JET ASDEX-U. The new JET helium points are the squares.